Chemical Bonding beyond the Fingerprints: A Quantitative Measure of Tetrahedral-sp^3 Geometries in Amorphous Phase Change Alloys

M. Micoulaut
Laboratoire de Physique Théorique de la Matière Condensée,
Université Pierre et Marie Curie, 4 Place Jussieu, F-75252 Paris Cedex 05, France

K. Gunasekera, S. Ravindren, and P. Boolchand
School of Electronics and Computing Systems, College of Engineering and Applied Science,
University of Cincinnati Cincinnati, OH 45221-0030, USA
(Dated: May 25, 2014)

Phase change or Ovonic memory technology has gained much interest in the past decade as a viable solution for the rapid increase in the demand for memory storage. This unique technology, first proposed by S. Ovshinsky in 1968, is based on storing information on crystalline and amorphous phases of a material. Most common phase change materials (PCMs) use chalcogenide alloys such as the $Ge_2Sb_2Te_5$ (GST225). However, while the structure of its crystalline phase is relatively well characterized as consisting of a rhombohedrally distorted rock-salt lattice, the corresponding amorphous phase remains still poorly understood. Here, we show that ^{119}Sn Mössbauer spectroscopy and angular constraint counting of simulated structures can provide a quantitative measure of sp^3 tetrahedral fraction of Ge opr Si cation in amorphous phase change binary tellurides Ge_xTe_{1-x} and Si_xTe_{1-x}. This represents the first quantitative estimate of such local structures, and reveals the fraction to be nearly 50 %, and to evolve with fraction x of the Group IV cation.

PACS numbers: 61.43.Fs ,
Keywords:

Phase change phenomenon involves a transition between a crystalline conducting state and an amorphous semiconducting one [1, 2], with attendant changes in electronic density of states and band gap. It has, therefore, been recognized that typical structural motifs (tetrahedra, octahedra) should play an important role in phase switching phenomena because of a change in nature of chemical bonding reflected by different electronic orbitals. The sp^3 hybridized tetrahedra, typical of covalent semiconductors, involves for instance only s electrons whereas an octahedral (s,p) bonding facilitate conduction. The local structure of such phase-change tellurides has been revealed from extended x-ray absorption fine structure (EXAFS) experiments [3, 4], and one has found that Ge atoms actually switch from a 6-fold octahedral coordination in the crystalline phase to a 4-fold coordination in an amorphous one.

The nature of this 4-fold Ge, whether a pyramidal (i.e. "*defect-octahedral*", DO) or a tetrahedral (T) unit, and its fraction, has been debated, and still remains unresolved. In addition, some conclusions based on EXAFS [5] and Reverse Monte Carlo simulations [6] have contradicted each other [3, 4]. This may simply result from uncontrolled sample processing [7] or deposition methods [8, 9] which can dramatically affect the physical behavior including the local structure. First Principles Molecular Dynamics (FPMD) simulations have been used to provide additional information [10–13] on the atomic coordination and geometry, and these have shown that the Te-coordination is larger than 2, whereas most of Ge is 4-fold with a finite fraction being sp^3 tetrahedral. However, the way this fraction is computed remains largely qualitative. Akola and Jones [10] assign tetrahedral character if all Ge-centred bond angles are greater than 100^o but this must obviously give rise to some uncertainties given that bond angles involved in the two geometries (DO and T, 90^o and 109^o) are close, and display distributions leading to a possible overlap. Alternatively, Raty and co-workers [11] used a bond-length argument in $Ge_1Sb_2Te_4$, remarking that the fourth-neighbor distribution of a Ge atom is bimodal, depending on wether it is three- or four-fold (tetrahedrally) coordinated. Finally, Caravati et al. [13] calculate a local order orientational order parameter distribution that reveals tetrahedral character [14] but the integration of this distribution that yields the estimate depends unfortunately on the integration boundaries.

Fingerprints of tetrahedral geometries have also been recently provided using either simulated Raman spectra [15] or X-ray Absorption Near Edge Structure spectroscopy [16] but the question of finding an explicit signature, and a quantitative measure of sp^3 tetrahedral Ge as a function of thermodynamic conditions (e.g. composition) in phase-change tellurides remains a largely open issue.

In the present Letter we address the *central* question of the nature of structural motifs and chemical bonding by investigating two binary amorphous tellurides, Ge_xTe_{1-x} and Si_xTe_{1-x} with $x \leq 20\%$. We propose two new methods in the context of phase change materials, an experimental and a theoretical one, that can determine without ambiguity the nature of the local structures (different geometry), their fraction, and their evolution under moderate compositional changes in the amorphous phase. Compared to previous experimental and theoretical studies, the present results mark compelling progress in the characterization of the topology of phase-change materials given that, ultimately, it is the signature of local structures and their fraction that controls functionality. We find that at low Ge and Si content (x=14-15%), both Si-Te

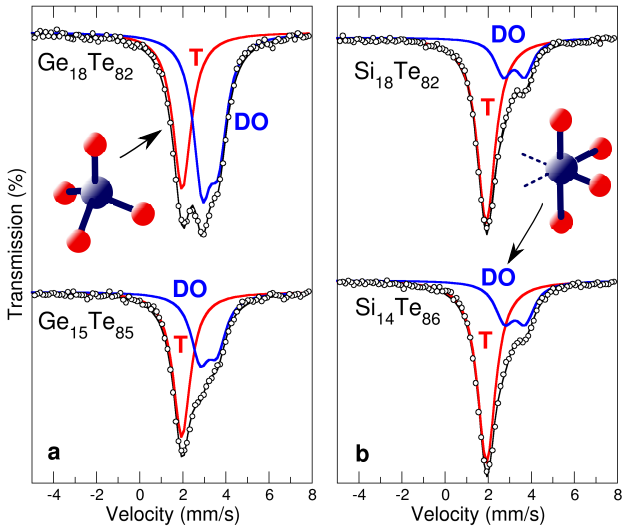

Figure 1: ^{119}Sn Mössbauer spectra of amorphous Ge_xTe_{1-x} (a) and Si_xTe_{1-x} at selected compositions. According to reference compounds, spectra can be deconvoluted into two sites T, tetrahedral (red), and DO (pyramidal, blue), the latter being schematically represented by an octahedral site with two vacancies.

and Ge-Te binary are dominated by sp^3 tetrahedral fractions in the 55-70% range. However, with only a slight increase of x=18%, in the Ge-Te binary, the sp^3 tetrahedral fraction dramatically lowers to near 42% with Ge atoms predominantly found in an octahedral geometry. On the other hand, in the Si-Te binary, the sp^3 tetrahedral fraction displays the opposite behavior, and increases up to $\simeq$ 92 % for x=20 %. These estimates established from a direct measurement (Mössbauer spectroscopy), and qualitatively recovered from the simulation, unravels the central role played by sp^3 tetrahedral motifs and provides, given the abundance of such structural motifs, support to phenomenological models of the phase change phenomenon [3]. Taken together, these results allow reconsidering in a rather deep and quantitative fashion the local structure of amorphous tellurides, while also revealing important implications for the phase change mechanism itself.

We rely on ^{119}Sn Mössbauer spectroscopy that allows for a detection of local structures *via* the nuclear hyperfine structure [17] (δ-isomer shift, and Δ-quadrupole splitting), and leads to a direct observation of site geometry. For the theory part, we use First Principles Molecular Dynamics (FPMD) simulations. Details on the experiments and on the obtained structural properties of the amorphous telluride models, can be found in the supplementary material section.

We first focus on the experimental signature. The local environment of Ge and Si has been probed using a novel characterization technique in the context of phase change materials - ^{119}Sn Mössbauer spectroscopy [17]. One dopes traces ($\simeq$1 wt%) of ^{119}Sn by reacting nearly 100 % isotopically enriched pure elemental Sn in the glass of interest. In trace amounts, *isovalent* Sn will replace Si and Ge local environments in the network, and reproduce the Group IV atom local geometry and chemical bonding. When Sn is in a sp^3-tetrahedral bonded state as a dilute substituent in c-Si, one observes a narrow Mössbauer resonance (Γ=0.80 mm/s to be compared with the Heisenberg principle determined natural linewidth of 0.69) with unique chemical shift of δ=1.65$\pm$0.02 mm/s with respect to Sn^{4+} (see spectra in Suppl. Material), this shift being characteristic of tetrahedrally coordinated Sn. Similarly, the Sn^{2+} oxidation state is found in crystalline SnTe which has an octahedral geometry as in GeTe [2], as revealed by a Mössbauer resonance at an isomer shift of δ=3.33$\pm$0.02 mm/s. Furthermore, since there are no vacancies in this perfect rocksalt-type structure of two Sn- and Te-sublattices, no quadrupole splitting is observed [17] which indicates presence of a octahedral coordination, i.e. the absence of vacancies in the immediate environnement of Sn.

Table I: Experimentally measured (Expt.) and calculated (Simul.) fraction η_T (in %) of tetrahedral sites in amorphous Ge-Te and Si-Te with changing content.

	$Ge_{10}Te_{90}$	$Ge_{15}Te_{85}$	$Ge_{17}Te_{83}$	$Ge_{18}Te_{82}$	$Ge_{20}Te_{80}$
Expt.		57.0$\pm$1.1	57.9$\pm$1.2	41.6$\pm$0.8	
Simul.	62.3$\pm$3.4	65.4$\pm$2.0			54.6$\pm$1.6
		$Si_{14}Te_{86}$	$Si_{16}Te_{84}$	$Si_{18}Te_{82}$	$Si_{20}Te_{80}$
Expt.		69.9$\pm$1.4	73.6$\pm$1.5	74.2$\pm$1.5	
Simul.		87.3$\pm$2.9			91.8$\pm$2.8

Figure 1 shows the Mössbauer spectra of 2 selected compositions in each telluride system, and these can be deconvoluted into a singlet (red curve) with isomer shift $\delta_T \simeq$ 1.92(2) to 1.98(2) mm/s range, and a doublet (blue curve) with an isomer shift, $\delta_{DO} \simeq$ 3.17(2) to 3.24(2) mm/s range, and a quadrupole splitting of $\Delta \simeq$0.73(3) to 1.08(3) mm/s range, but with observed linewidths, $\Gamma \simeq$0.94(3) to 1.07 mm/s suggestive of rather well defined local environments. The minimum observable natural (uncertainty principle) linewidth is 0.69 mm/s. The singlet δ_T close to the chemical shift of c-Si, is a clear indication of the presence of tetrahedral (T) coordination and sp^3 bonding, similar to what is observed in corresponding selenides [18]. The resonance doublet centred at δ_{DO} highlights the presence of Sn in octahedral sites. In contrast with a single resonance peak found in c-SnTe, in the amorphous phases one observes an electric field gradient responsible for the doublet Δ, which arises from the fact that Sn is in a *defect* octahedral configuration given that a majority of Ge is four-fold coordinated (see below, and Ref. [19]). Once the integrated area of T and DO resonances is calculated, one obtains the fraction of T and DO local structures, and the fraction η_T of tetrahedra (Table I). The two binary tellurides actually display quite different behavior. In the Ge-Te, the DO-pyramidal geome-

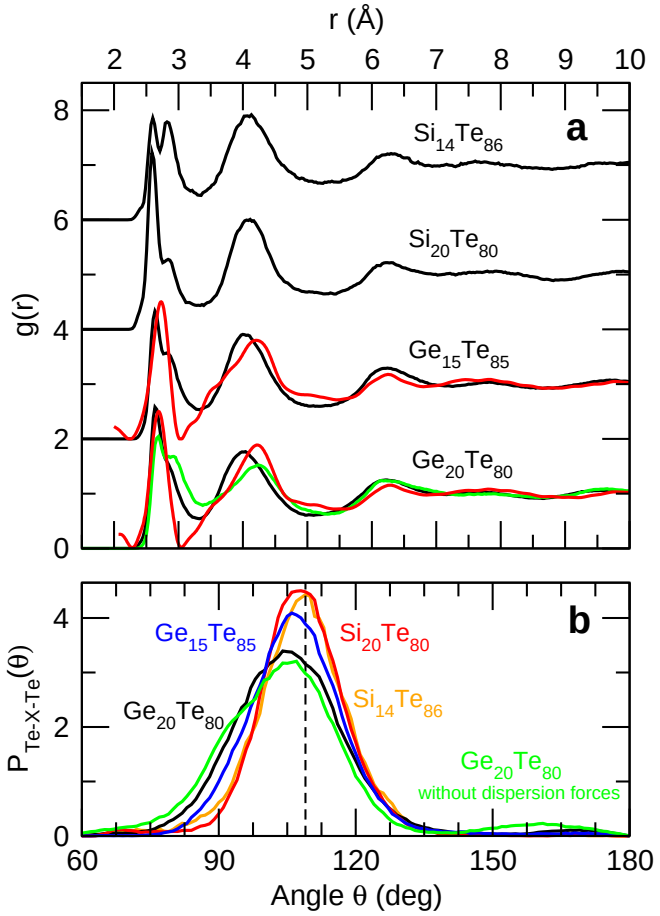

Figure 2: (Color online) a) Calculated total pair correlation function g(r) of $Ge_{15}Te_{85}$, $Ge_{20}Te_{80}$, $Si_{14}Te_{86}$ and $Si_{20}Te_{80}$, compared to the corresponding experimental function from neutron diffraction (red, [19]). The green curve corresponds to a simulation that does not take into account the correction due to dispersion forces [20]. b) Simulated Te-X-Te (X=Ge,Si) bond angle distribution in amorphous $Ge_{15}Te_{85}$, $Ge_{20}Te_{80}$, $Si_{14}Te_{86}$ and $Si_{20}Te_{80}$. The broken vertical line corresponds to the angle of 109^o.

try, while representing minority sites at x=15%, grows rapidly with increasing x and becomes the dominant motif close to $Ge_{20}Te_{80}$. This behavior is in sharp contrast to the case of the Si-based analogue, which displays already a large fraction of T sites at low (14%) Si content (69.9%), and with growing x, this fraction increases mildly to 74.2% at $Si_{18}Te_{82}$. The opposite trends between Ge-Te and Si-Te alloys can be related to the known crystalline polymorphs (GeTe and Si_2Te_3) that dominate the local structure at higher modifier content, and which display for the Group IV atom an octahedral and a tetrahedral environment, respectively [21, 22].

The present findings on $\eta_T(x)$ are actually qualitatively consistent with those determined from models of amorphous Ge-Te and Si-Te using our FPMD simulations, which reproduce quite accurately the structure [19] in real space (Fig. 2a), and lead to coordination numbers r_{Ge}=4.16, r_{Si}=3.97, and r_{Si}=3.99 for $Ge_{20}Te_{80}$, $Si_{14}Te_{86}$ and $Si_{20}Te_{80}$, respectively.

The bond angle distribution around Ge and Si (Te-Ge-Te and Te-Si-Te) already shows the difference in geometry between the two systems (Fig. 2b) because $Si_{14}Te_{86}$ and $Si_{20}Te_{80}$ display a distinct peak at 109^o in the Te-Si-Te bond angle distribution, indicative of the tetrahedral geometry. Both $Ge_{15}Te_{85}$ and $Ge_{20}Te_{80}$ have their bond angle distribution shifted to lower angles (95-100^o), together with a small contribution at 160^o, which indicate a predominantly DO geometry for Ge. As already noticed before [10, 11], these "*global*" bond angle distributions do not permit accessing the precise population of tetrahedra.

To detect and calculate quantitatively their population, we use algorithms that enumerate angular topological constraints [23], but in contrast with a previous work [24], we do not perform an initial search of tetrahedral units using a bond length argument [11], and fully rely on angular excursions that are computed on-the-fly. We follow individually over the simulation trajectory the N_a=N(N-1)/2 angles defined by a set of N first neighbors around a central Ge or Si atom (in the following, we choose N=6). Over the simulated trajectory (i.e. with time), these individual angles define a partial bond angle distribution out of which a mean $\bar{\theta}$ and a standard deviation σ_θ can be computed for *each* Ge/Si atom of the system. If the number of low standard deviations σ_θ around an atom is six, a tetrahedron is identified because this geometry is defined by six rigid angles [10] that give rise to corresponding low standard deviations (Fig. 3a). In this respect, this dichotomic selection rule differs from previous methods that relie on continuous structural parameters. Averages over the system then leads to a precise fraction η_T of Ge or Si tetrahedra that compares favourably to the experimental estimate (Table I). Once the six angular excursions are identified, Figure 3b shows indeed that the associated system-averaged mean angle is equal to $\langle\bar{\theta}\rangle \simeq 109^o$ (blue arrows), and a corresponding bond angle distribution (Fig. 3c) peaks at 109^o. Both Si-Te and Ge-Te systems display a similar distribution, the latter being identical to the corresponding Se-Ge-Se distribution [23] in the isochemical $Ge_{20}Se_{80}$ where η_T=100%. The similarity between the Si- and Ge-based bond angular distribution of T-sites is also consistent with the identical isomer shift δ_T found in Mössbauer spectroscopy (Fig. 1a and b) for Ge_xTe_{1-x} and Si_xTe_{1-x} (red)

The remaining non-tetrahedral (nT) Ge and Si geometry can now also be characterized. In $Ge_{20}Te_{80}$, only three angles are found to have small angular excursions ($\sigma_\theta \simeq$ 10-17^o, red bars/angles for $_1Ge_2$(n=1), $_1Ge_3$(n=2) and $_2Ge_3$(n=6), Fig. 3a), and are associated with the first three neighbors of Ge at distances of about 2.69$\pm$0.07Å, and with angles found at $\bar{\theta} \simeq$ 98^o (red arrows, Fig. 3b). This defines a pyramid with a triangular basis having the Te-Te bonds as edges, and a Ge at the remaining vertex, similar to the pyramidal geometry found in As_2Se_3 for which 3 rigid angles are obtained [25]. This leads to a similar bond angle distribution (orange curve, Fig. 3c). However, in the first coordination shell a fourth neighbor (Te) is found at a slightly larger distance (2.96 Å), and the associated angles ($_1Ge_4$(n=3), $_2Ge_4$(n=7) and $_3Ge_4$(n=10)) exhibit

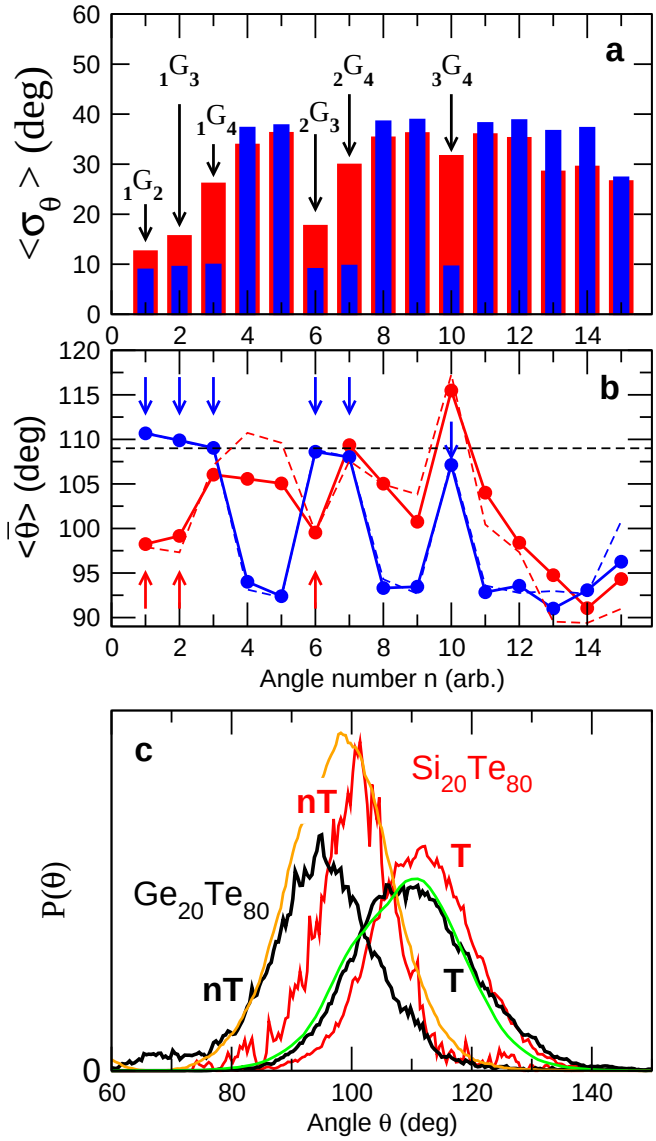

Figure 3: a) Standard deviation $\langle\sigma_\theta\rangle$ for arbitrary angle numbers n ($0<n<N_a=15$) around Ge atoms in amorphous $Ge_{20}Te_{80}$ split into two categories: Ge atoms having 6 low σ_θ's (blue), and Ge atoms having not such six σ_θ's (red). The arrows indicate the relevant angles $_kGe_m(n)$ serving for the discussion. Here m and $k < m$ are the Te neighbors, and labelled according to their distance with respect to the central Ge atom. b) Corresponding Ge-centred angles $\langle\theta\rangle$. The broken lines correspond to the $Ge_{15}Te_{85}$ compound. Colored arrows indicate angles which can be considered as rigid (because of panel a) and which serve to cross-check the angles ($\simeq 109^o$ or $\simeq 98^o$) of the local geometries. c) Bond angle distribution of identified tetrahedral (T)/non-tetrahedral (nT) Ge and Si in $Ge_{20}Te_{80}$ (black) and $Si_{20}Te_{80}$ (red). The green curve corresponds to the Se-Ge-Se bond angle distribution in the isochemical $Ge_{20}Se_{80}$ [23], and the orange curve corresponds to the simulated Se-As-Se bond angle distribution of pyramidal As in amorphous As_2Se_3 [25].

much larger angular excursions (25-35^o, red bars/angles 3, 7 and 10, Fig. 3a) indicating a much softer geometry with corresponding angles found at 105-115^o (Fig. 3b). We recover similar results for the remaining $Ge_{10}Te_{90}$, $Ge_{15}Te_{85}$, and $Si_{14}Te_{86}$.

Having established the fraction η_T of such sp^3 tetrahedral structures, we then address the question of their occurence with decreasing temperature for a selected composition ($Ge_{20}Te_{80}$). An investigation at different liquid temperatures T (923 K, 823 K, 700 K) of $Ge_{20}Te_{80}$ shows that the the fraction η_T(T) does not follow the probability x_4(T) of finding a 4-fold Ge, the latter being found to increase with decreasing temperature, and grows from 45 % at 923 K to 77 % at 300 K. We find indeed that tetrahedra represent minority sites at 923 K (20 %) but then steadily increase down to room temperature where they represents the dominant motif (54.6 %, Table I).

Given the high content of tetrahedra for this compound (Fig. 1a, and Table I), an immediate consequence of the present findings is that changes in bonding and geometrical motifs should definitely play an important role in the phase change phenomenon. First, the conclusion traces back to a proposed mechanism [3] for the crystal-amorphous transition, related to the local switching (an "*umbrella flip*") of Ge atoms from an octahedral to a tetrahedral environment. This picture has been challenged in the literature from FPMD simulations disregarding dispersion forces but such simulations (as the green curve in Fig. 2) usually lead to a systematic overestimation of the Ge-Te bond lengths and Ge coordination numbers with respect to experiments [19]. They also lead to a significantly higher fraction as we have calculated η_T=23.4 % for $Ge_{20}Te_{80}$ that also manifest in a different shape for the total bond angle distribution (green curve, Fig. 2b). Simulations with dispersion corrections (black curve in Fig. 2) exhibit an increased agreement with experiments, and lead to reduced bond lengths thus promoting an increased tetrahedral bonding, a feature quite well established when bond lengths are followed during a controlled tetrahedral to octahedral conversion under pressure [26].

The determined bonding characteristics leads to even broader consequences. With an average number of (s,p) electrons usually larger than four, sp^3 hybridization in phase change materials seems unlikely at a first glance, as it should lead to a similar octahedral structure for both the crystalline and amorphous phases. Indeed, sp^3 tetrahedral geometries would involve occupied (but energetically unfavourable) sp^3 anti-bonding states, and lead to the absence of resonance bonding which seem to control [27] a certain number of electronic properties (e.g. contrast) for phase change applications. This seems consistent with the fact that the ease of phase switching is directly linked to small ionicity and a limited degree of hybridization [1], enabling resonance p-electron bonding to prevail. However, given the obsered large number of sp^3 hybridization found in the present Ge-Te binary, one is led to believe that only a fraction (1-η_T) of Ge atoms must be involved in such p-bond driven phase-change mechanism.

While we cannot further comment on popular phase-change alloys (e.g. GeTe or $Ge_2Sb_2Te_5$) given our investigated compositions, because of a large fraction of Ge being in sp^3 hybridization, only select number of atoms must obviously be subject to resonance bonding in order to drive the properties of e.g. the $Ge_{20}Te_{80}$ compound which has been found to exhibit [28] more promising switching temperatures (crystallization/melting) when compared with GeTe or the GST225, indicating that it may also be a competitive candidate for memory applications.

Acknowledgements: MM acknowledges support from Agence Nationale de la Recherche (ANR) (Grant No. ANR-11-BS08-0012), from the Franco-American Fulbright Commission, and International Materials Institute. PB acknowledges support from NSF grant DMR-08-53957.

[1] T. Hickel, J. Neugebauer, M. Wuttig, D. Lencer, M. Salinga, B.J. Grabowski, Nature Mater. **7**, 972 (2008).
[2] *Phase Change Materials and Applications*, S. Raoux, M. Wuttig Eds. (Springer, Berlin, 2008).
[3] A. V. Kolobov, P. Fons, A. I. Frenkel, A. L. Ankudinov, J. Tominaga, and T. Uruga, Nature Mater. **3**, 703 (2004).
[4] A. V. Kolobov, P. Fons, J. Tominaga, Appl. Phys. Lett. **82**, 382 (2003).
[5] D. A. Baker, M.A. Paessler, G. Lucovsky, S.C. Agarwal, P.C. Taylor, Phys. Rev. Lett. **96**, 255501 (2006).
[6] S. Kohara et al. Appl. Phys. Lett. **89**, 201910 (2006).
[7] K. Gunasekera, S. Bhosle, P. Boolchand, M Micoulaut, J. Chem. Phys. **139**, 164511 (2013).
[8] P. Jóvári, I. Kaban, J. Steiner, B. Beneu, A. Schops, M.A. Webb, Phys. Rev. B **77**, 035202 (2008).
[9] M. Krbal, A.V. Kolobov, P. Fons, J. Tominaga, S. Elliott, J. Hegedüs and T. Uruga, Phys. Rev. B **83**, 054203 (2011).
[10] J. Akola, R.O. Jones, Phys. Rev. B **76**, 235201 (2007).
[11] J.-Y. Raty, C. Otjacques, J. P. Gaspard, and C. Bichara, Solid State Sci. **12**, 193 (2010).
[12] J. Kalikka, J. Akola, R.O. Jones, S. Kohara, and T. Usuki, J. Phys. Cond. Matt. **24**, 015802 (2012).
[13] S. Caravati, M. Bernasconi, T. D. Kuehne, M. Krack, and M. Parrinello, Appl. Phys. Lett. **91**, 171906 (2007).
[14] P. L. Chau and A. J. Hardwick, Mol. Phys. **93**, 511 (1998).
[15] R. Mazzarello, S. Caravati, S. Angioletti, M. Bernasconi, and M. Parrinello, Phys. Rev. Lett. **104**, 085503 (2010).
[16] M. Krbal, A.V. Kolobov, P. Fons, K.V. Mitrofanov, Y. Tameroni, J. Hegedüs, S.R Elliott, and J. Tominaga, Appl. Phys. Lett. **102**, 111904 (2013).
[17] P. Boolchand in *Physical Properties of Amorphous Materials*, D. Adler, B.B. Schwartz, M.C. Steele Eds. (Plenum Press, New York, 1985), p. 221.
[18] P. Boolchand, P. Chen, M. Jin, B. Goodman and W. J. Bresser, Physica B **389**, 18 (2007).
[19] P. Jóvári, A. Piarristeguy, R. Escalier, I. Kaban, J. Bednarcik, A. Pradel, J. Phys. Cond. Matt. **25**, 195401 (2013).
[20] S. Grimme, J. Comput. Chem. **27**, 1787 (2006).
[21] S. Raoux, W. Welnic, D. Ielmini, Chem. Rev. **110**, 240 (2010).
[22] K. Ploog, W. Stetter, A. Nowitzki, E. Schönherr, Mater. res. Bull. **11**, 1147 (1976).
[23] M. Micoulaut, A. Kachmar, M. Bauchy, S. Le Roux, C. Massobrio, M. Boero, Phys. Rev. B **88**, 054203 (2013).
[24] M. Micoulaut, C. Otjacques, J-Y. Raty, C. Bichara, Phys. Rev. B **81**, 174206 (2010).
[25] M. Bauchy, M. Micoulaut, J. Non-Cryst. Solids **377**, 34 (2013).
[26] J. P. Itié, A. Polian, G. Calas, J. Petiau, A. Fontaine, and H. Tolentino, Phys. Rev. Lett. **63**, 398 (1989).
[27] K. Shportko, Nature Mater. **7**, 653 (2008).
[28] H. Jiang, K. Guo, H. Xu, Y. Xia, K. Jiang, F. Tang, J. Yin, and Z. Liu, J. Appl. Phys. **109**, 066104 (2011).